THE CYGNSS COHERENT END-TO-END SIMULATOR: DEVELOPMENT AND RESULTS

Hugo Carreno-Luengo[1], April Warnock[2], and Christopher S. Ruf[1]

[1]Climate and Space Sciences and Engineering Department, University of Michigan (UMich)
[2]SRI International
Ann Arbor, MI, United States of America (USA)
Email: {carreno,cruf}@umich.edu, {april.warnock}@sri.com

IGARSS 2022 - 2022 IEEE International Geoscience and Remote Sensing Symposium | 978-1-6654-2792-0/22/$31.00 ©2022 IEEE | DOI: 10.1109/IGARSS46834.2022.9884499

ABSTRACT

The CYclone Global Navigation Satellite System (CYGNSS) End-to-End Simulator (E2ES) is updated with a new module capable of accurately simulating coherent forward scattering from inland water bodies. This module uses a Global Navigation Satellite Systems Reflectometry (GNSS-R) model that can account for both coherent and incoherent scattering due to small scale surface roughness. The model is developed based on the Huygens-Kirchhoff principle. One principle application is to support the development of wetland extent retrieval algorithms over heterogenous scenes. In this abstract, a water mask corresponding to a lake surrounded by mountains and vegetation is considered. A modeled time series of reflected power is generated and results are compared to actual CYGNSS raw IF data. The final goal is to support scientific studies related to the capabilities of CYGNSS for inland water body monitoring.

Index Terms— CYGNSS, GNSS-R, E2ES, land surfaces, inland water bodies, coherent and incoherent scattering

1. INTRODUCTION

CYGNSS is the NASA 8-microsatellite constellation L-band passive multi-bistatic radar that uses GNSS signals as signals of opportunity [1,2]. It was first proposed for ocean surface wind speed estimation over tropical cyclones [1,2]. Land surface applications i.e. soil moisture content, biomass, inland waters were explored later [3]. CYGNSS is the first operational GNSS-R [4,5] spaceborne mission.

The use of CYGNSS for detection and monitoring of inland water bodies has shown a strong performance, even over tropical forests (Fig. 1). The signal dynamic range is high enough so as to detect even small water bodies such as small rivers [7-9].

The foundation of such strong sensitivity is in the nature of the coherent scattering [10-12]. The behaviuor of the composite scattering from small smooth regions interspersed within a larger rough terrain was investigated in [13]. Here, we present details of the numerical implementation and the strategy to account for both the incoherent scattering from land and the coherent scattering from inland water bodies. First results are also depicted.

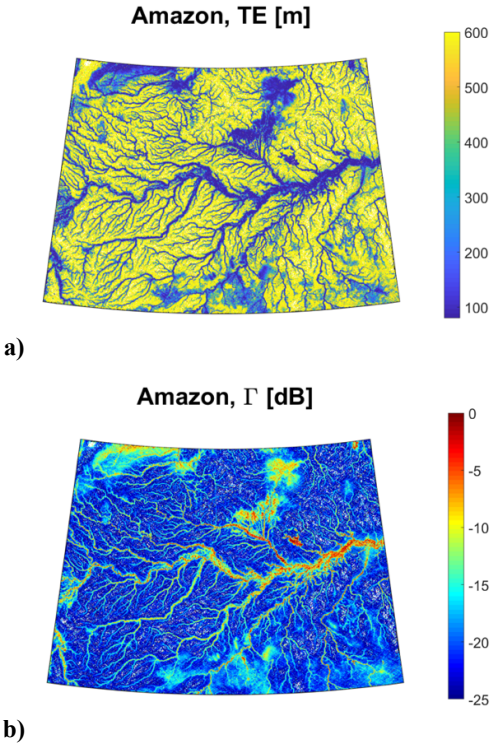

Fig. 1. CYGNSS capability to detect inland water bodies over Amazon tropical rainforests: a) Trailing Edge TE width, b) reflectivity Γ. Small inland water bodies are detected even with very high Above-Ground Biomass (AGB) [6].

This paper is organized as follows. Section 2 summarizes the GNSS-R model. Section 3 describes the updated E2ES. Section 4 provides details of the numerical implementation. First resuls are included in Section 5. Finally, preliminary conclusions are drawn in Section 6.

2. GNSS-R SCATTERING MODEL

A GNSS-R surface scattering model based on the Huygens-Kirchhoff principle was proposed and validated using spaceborne data processed with the CYGNSS raw IF processor [13]. This model has the ability to account for both coherent and incoherent scattering, attenuation effects by vegetation, and the impact of the incidence angle.

Under the Huygens-Kirchhoff principle, power Delay Doppler Maps (DDMs) can be expressed as follows [13]:

$$\langle |Y(\tau,f)|^2 \rangle = \upsilon P_t G_t \frac{\lambda^2 G_r}{4\pi} \left| -jk \iint \frac{2cos\theta_i X(\tau,f)}{4\pi R_t R_r} \sqrt{\gamma |R|^2 e^{-(2k\sigma cos\theta_i)^2}} e^{jk(R_t+R_r)} dA \right|^2 \quad (1)$$

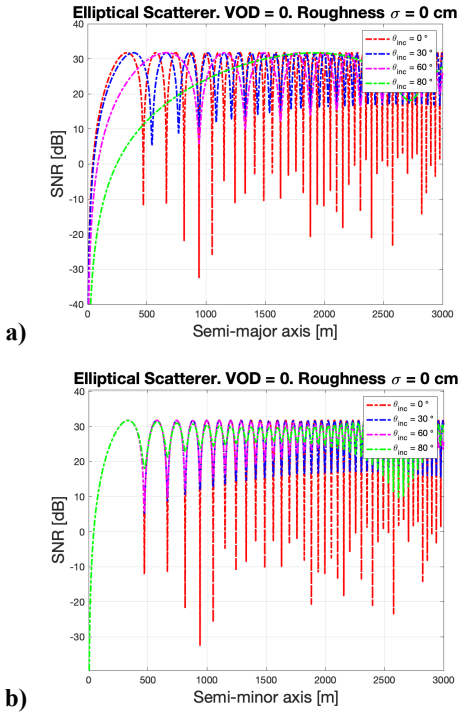

a)

b)

Fig. 2. Simulated Signal-to-Noise Ratio (SNR) of the coherent scattering term as a function of the axes of a elliptical scatterer: a) semi-major axis, and b) semi-minor axis. The results are evaluated as a function of the incidence angle.

where υ is is the characteristic free space wave impedance ~ 120π, P_t is the power of the transmitted Global Positioning System (GPS) signals, G_t is the gain of the transmiting antenna, G_r is the gain of the receiving antenna, λ is the signal wavelength, k is the angular wavenumber, θ_i is the incidence angle, X is the Woodward Ambiguity Function (WAF), τ is the delay of the signal from the transmitter to the receiver, f is the Doppler , R_r and R_t are, respectively, the ranges from the receiver and the transmitter to the specular reflection point, γ is the transmissivity of the vegetation, R is the complex Fresnel reflection coefficient, and σ is the surface height standard deviation (related to small-scale surface roughness).

Results demonstrated the impact of higher order Fresnel zones (Fig. 2) on the total coherent reflected power as collected by a GNSS-R sensor, showing ringing fluctuations in the reflected power near high contrast boundaries. This effectively determines the spatial resolution of GNSS-R over heterogenous areas. In the case of an elliptical sccaterer, we can see perfect ringing fluctuations (Fig. 2). On the other hand, in the case of a circular scatterer, the geometry of the water mask cuts off the constructive/destructive interference of the higher order Fresnel zones [13].

3. UPDATED CYGNSS E2ES

The CYGNSS E2ES has been updated with a new coherent module using the electromagnetic model previously described. As such, in addition to the incoherent scattering module previously included in the E2ES, now the coherent one can also be simulated.

The most relevant and useful applications for the updated E2ES will probably be for cases where there are both coherent and incoherent components to the scattered signal received by CYGNSS, and where the exact geometry of the coherently scattering surface (e.g. the boundaries of the inland water bodies) have complicated shapes. The updated CYGNSS E2ES can be tuned to different specific scenarios by varying the water mask used.

Here, the considered scenario is an inland water body surrounded by rough surface terrain and thick vegetation cover. The land surface contribution is dominated by the incoherent scattering, which is provided by the E2ES incoherent scattering module $\langle |Y_{land,inc}(\tau,f)|^2 \rangle$. The inland water contribution is dominated by the coherent scattering, which is provided by the E2ES coherent scattering module $\langle |Y_{water,coh}(\tau,f)|^2 \rangle$. This module has the ability to account for the non-negligible incoherent scattering over inland water bodies due to small scale surface roughness, which can be generated by the winds.

The output of the updated E2ES is as follows:

$$\langle |Y_{total}(\tau,f)|^2 \rangle = \langle |Y_{land,inc}(\tau,f)|^2 \rangle + \langle |Y_{water,coh}(\tau,f)|^2 \rangle \quad (2)$$

This strategy allows us to account for the contribution of the incoherent scattering within the large glistening zone, but also the impact of the inland water bodies, including the effect of the higher order Fresnel zones.

4. NUMERICAL IMPLEMENTATION

Theoretically, the integral in eqn. (1) should extend over an infinite surface when a significant number of complete Fresnel zones contribute to the re-radiation pattern from the surface. This approach is not valid in a real scenario because the scattering decreases quickly as the scatterers are farther away from the nominal specular point. This section revisits the conclusion that 20 km x 20 km and 1 m [13] are acceptable domain size and grid size values to use.

The accuracy of the numerical implementation depends on various discrete approximations, including the grid size and the domain size of the water mask inputted to the model.

The requirements differ for the incoherent and coherent scattering components. The majority of coherent scattering signal is received from the first few Fresnel zones, while the incoherent scattering is more diffuse and received from the entire glistening zone. Hence, the coherent scattering module is expected to require a smaller domain size over which contributions to the received signal are considered. However, because the scattering contribution over the smooth water bodies retains phase coherence, the coherent scattering calculations are more sensitive to the calculated propagation distances, so a smaller grid size is required to resolve this component of the signal. By constrast, incoherent scattering over the rough land surface is decorrelated to such a degree that the phase of scattered signals from different facets can be considered random and a larger grid size is sufficient to resolve the received signal. In order to increase model efficiency in light of the differences in grid requirements between the coherent and incoherent scattering components, the two modules are run on separate grids and the resulting signals are added together to get the total received signal.

To determine the required bounds on domain and grid sizes, a synthetic lake case was constructed as shown in Fig. 3. Satellite geometry was taken from a CYGNSS raw IF overpass obtained on July 30th, 2021, corresponding to $\theta_i \sim$ 10°. The lake is a 5 km x 5 km square located in the center of the specular point track, oriented so that the edges are aligned with the specular point track. The coherent scattering model was run for a range of domain and grid sizes, using a 50 ms time step. Figure 4 shows the results of the grid study for the coherent scattering module for varying grid size over a 20 km x 20 km domain (Fig. 4a), and for varying domains with a 1 m grid size (Fig. 4b). The figures are zoomed in to focus on the signal behavior over the water body. In all cases, the signals are essentially identical when the specular point is directly over the lake (~2.5-3.5 seconds into the simulation). In order to accurately capture the leading and trailing edges of the signal, however, the results indicate that a domain size of 10 km x10 km and a grid resolution of 2 m are sufficient for this geometry. Note that for larger inclination angles, these values may need to be adjusted.

The incoherent domain size is constrained by the WAF, which extends roughly 20 km x 20 km from the specular point for a nominal geometry. Fig. 5 shows results of the incoherent scattering module for the track shown in Fig. 3, for varying grid resolutions with a 20 km x 20 km domain size (Fig. 5a), and for varying domain sizes with a fixed grid size of 40 m (Fig. 5b). Fig. 5a indicates that for the incoherent scattering signal component, a grid of 100 m is sufficient, while Fig. 5b shows that a domain size of 40 km x 40 km leads to convergence. As with the coherent scattering compenent, greater inclination angles may impact these limits.

5. APPLICATION WATER MASK: LAKE SCENARIO

The performance of the updated E2ES is demonstrated with a comparison of CYGNSS raw IF data over Lake Ilopango in El Salvador to the simulated signal. Lake Ilopango is a roughly 8 km x 11 km volcano crater lake that is surrounded largely by dense vegetation. The raw IF for this

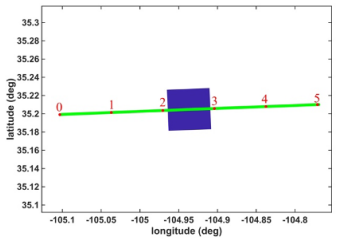

Fig. 3. Synthetic 5 km x 5 km lake aligned with an actual CYGNSS raw IF overpass from July 30th, 2021. The blue square represents the water body, the green line denotes the specular point track on the ground, and the numbers denote the time in seconds relative to the start of the model simulation.

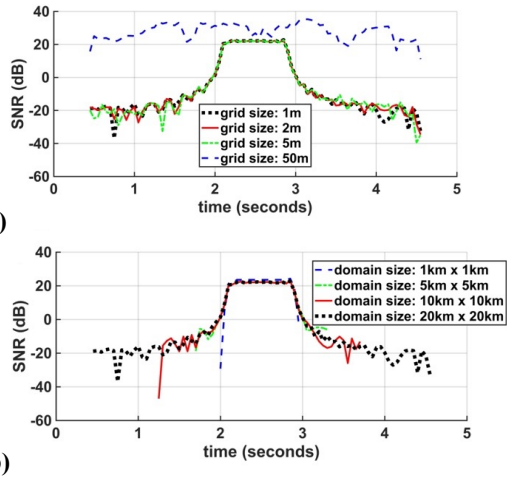

Fig. 4. Grid study results for the coherent scattering component for: a) varying grid size over a 20 km x 20 km scattering area, and b) varying scattering areas with a 1 m grid resolution.

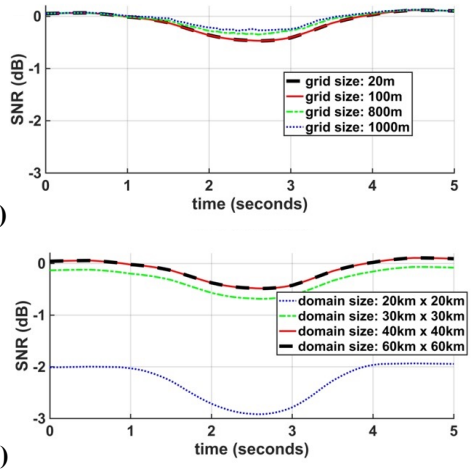

Fig. 5. Grid study results for the incoherent scattering compenent for: a) varying grid size, with the domain size fixed at 20 km x 20 km, and b) varying domain size, with the grid size fixed at 40 m.

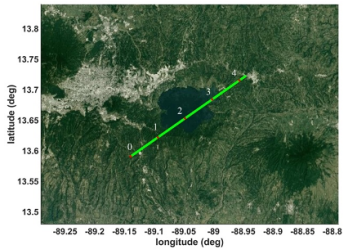

Fig. 6. CYGNSS specular point track (green line) over Lake Ilopango. Numbers respresent seconds from start of the simulation.

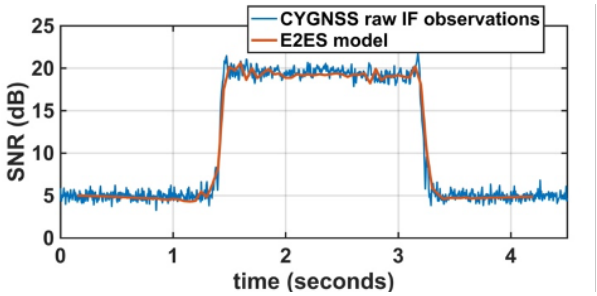

Fig. 7. Simulated (red line) vs actual (blue line) signal over Lake Ilopango.

case was collected on August 22th, 2019 and processed with 50 ms incoherent averaging at a 5 ms time step. The spatial resolution and scattering area for the water mask were specified according to the optimal values determined in Section 4. The specular point track is shown in Fig. 6, overlaid on GoogleEarth imagery of Lake Ilopango collected in 2021.

The grid and domain sizes for the incoherent and coherent scattering model components were defined as 2 m and 10 km x10 km for the coherent scattering component, and 100 m and 40 km x 40 km for the incoherent scattering component, respectively. These values were selected based on the convergence study results shown in Section 4.

The updated E2ES results for the Lake Ilopango overpass are shown in Fig. 7, where the true signal is in blue and the simulated signal is in red. The simulation was run at a 50 ms time step, hence the smoother signal over the coherent scattering dominant portion of the domain (over the lake) compared to the actual signal. The smoothness of the incoherent signal dominant portion of the specular point track to the left and right of the water body is also the result of using homogenous estimates for the land surface properties, while the true signal reflects receiver noise, speckle etc that the true land surface contains. Overall, the match between the observed and simulated signals is excellent and demonstrates the capability of the updated E2ES to model a complex inland scene.

6. CONCLUSIONS

The CYGNSS E2ES has been updated and now has the capability of simulating complex overland scenes that contain both coherent and incoherent scattering, whereas the original model was constructed to model ocean surface scenes dominated by incoherent scattering. The coherent and incoherent scattering components require different grid and domain sizes, and hence the two modules are run in parallel and the resulting signal components combined to derive the total signal. Preliminary grid convergence studies indicate that a 10 km x 10 km domain and a 2 m grid size is sufficient for the coherent scattering component, while a 40 km x 40 km domain and 100 m grid size is sufficient for the incoherent scattering model needs.

Further studies will be conducted to assess the applicability of these domain and grid bounds to other geometries, surface conditions, etc. We have applied the E2ES to an actual CYGNSS overpass on Lake Ilopango in 2019 and the results indicate excellent agreement between the observed and modeled signals.

7. REFERENCES

[1] C. Ruf, M. Unwin, J. Dickinson, R. Rose, D. Rose, M. Vincent, and A. Lyons, "CYGNSS: Enabling the Future of Hurricane Prediction [Remote Sensing Satellites]," IEEE Geoscience and Remote Sensing Magazine, vol. 1, no. 2, pp. 52-67, 2013.

[2] C. Ruf, et al., "CYGNSS Handbook," Ann Arbor, MI, Michigan Pub., ISBN 978-1-60785-380-0, 2016.

[3] H. Carreno-Luengo, J.A. Crespo, R. Akbar, A. Bringer, A. Warnock, M. Morris, and C. Ruf, "The CYGNSS Mission: On-Going Science Team Investigations," MDPI Remote Sensing, vol. 13, no. 9, pp. 1814, May 2021.

[4] M. Martin-Neira, "A Passive Reflectometry and Interferometry System (PARIS): Application to Ocean Altimetry," ESA J., vol. 17, pp. 331-355, Jan. 1993.

[5] J.L. Garrison, A. Komjathy, V.U. Zavorotny, and S.J. Katzberg, "Wind Speed Measurement Using Forward Scattered GPS Signals," IEEE Transactions on Geoscience and Remote Sensing, vol. 40, no. 1, pp. 50-65, 2002.

[6] H. Carreno-Luengo, G. Luzi, and M. Crosetto, "Above-Ground Biomass Retrieval over Tropical Forests: a Novel GNSS-R Approach with CYGNSS," MDPI Remote Sensing, vol. 12, no. 9, pp. 1368, 2020.

[7] C. Chew, J.T.Reager, and E. Small, "CYGNSS Data Map Flood Inundation During the 2017 Atlantic Hurricane Season," Scientific Reports, vol. 8, pp. 1-8, 2017.

[8] A. Warnock and C. Ruf, "Response to Variations in River Flowrate by a Spaceborne GNSS-R River Width Estimator," MDPI Remote Sensing, vol. 11, no. 20, pp. 2450, 2019.

[9] M. M Al-Khaldi, J. T Johnson, S. Gleason, C. C. Chew, C. Gerlein-Safdi, R. Shah, and C. Zuffada, "Inland Water Body Mapping Using CYGNSS Coherence Detection," IEEE Transactions on Geoscience and Remote Sensing, vol. 59, no. 9, pp. 7385-7394, 2021.

[10] H. Carreno-Luengo, and A, Camps, "First Dual-Band Multi-Constellation GNSS-R Scatterometry Experiment over Boreal Forests from a Stratospheric Balloon," IEEE Jounal of Selected Topics in Applied Earth Observations and Remote Sensing, vol. 9, no. 10, pp. 4743-4751, 2015.

[11] H. Carreno-Luengo and A. Camps, "Unified GNSS-R Formulation Including Coherent and Incoherent Scattering Components," in Proc. of the 2016 IEEE IGARSS, pp. 4815-4818, Beijing, China, July 2016.

[12] A. Camps, "Spatial Resolution in GNSS-R Under Coherent Scattering," IEEE Geoscience and Remote Sensing Letters, vol. 17, no. 1, pp. 32-36, 2019.

[13] H. Carreno-Luengo, C. Ruf, A. Warnock, and K. Brunner, "Investigating the Impact of Coherent and Incoherent Scattering Terms in GNSS-R Delay Doppler Maps," in Proc. of the 2020 IEEE IGARSS, pp. 6202-6205, Hawaii, USA, July 2020.

Acknowledgements

This research was supported in part by the NASA Science Mission Directorate contract 80LARC21DA003 with the University of Michigan.